Eppinga RD, Peng IF, Lin JL et al.Opposite effects of overexpressed myosin Va or heavy meromyosin Va on vesicle distribution, cytoskeleton organization, and cell motility in nonmus…

ARTICLE *in* CELL MOTILITY AND THE CYTOSKELETON · MARCH 2008

Impact Factor: 4.19 · DOI: 10.1002/cm.20255 · Source: PubMed

Cell Motility and the Cytoskeleton 65: 197–215 (2008)

Opposite Effects of Overexpressed Myosin Va or Heavy Meromyosin Va on Vesicle Distribution, Cytoskeleton Organization, and Cell Motility in Nonmuscle Cells

Robbin D. Eppinga, I-Feng Peng, Jenny Li-Chun Lin, Chun-Fang Wu, and Jim Jung-Ching Lin*

Department of Biological Sciences, University of Iowa, Iowa City, Iowa

Myosin Va, an actin-based motor protein that transports intracellular cargos, can bundle actin in vitro. Whether myosin Va regulates cellular actin dynamics or cell migration remains unclear. To address this, we compared Chinese Hamster Ovary (CHO) cells that stably express GFP fused to either full length mouse myosin Va (GFP-M5) or heavy meromyosin Va (GFP-M5Δ). GFP-M5 and GFP-M5Δ co-immunoprecipitate with CHO myosin Va and serve as overexpression of wild-type and dominant negative mutants of myosin Va. Compared to non-expressing control cells, GFP-M5-overexpressing cells have peripheral endocytic vesicles, spread slowly after plating, as well as produce robust interior actin stress fibers, myosin II bundles, and focal adhesions. However, these cells display normal cell migration and lamellipodial dynamics. In contrast, GFP-M5Δ-expressing cells have perinuclear endocytic vesicles, produce thin interior actin and myosin bundles and contain no interior focal adhesions. In addition, these cells spread rapidly, migrate slowly and display reduced lamellipodial dynamics. Similarly, neurite outgrowth is compromised in neurons cultured from transgenic *Drosophila* that express M5Δ-dsRed and in neurons cultured from *Drosophila* that produce a tailless version of endogenous myosin V. Together, these data suggest that myosin Va overexpression induces actin bundles in vivo whereas the tailless version fails to bundle actin and disrupts cell motility. Cell Motil. Cytoskeleton 65: 197–215, 2008.

Key words: cell migration; stress fiber; wound-healing; neurite outgrowth; unconventional myosin; cell shape; CHO cells; *Drosophila* neurons; vinculin

INTRODUCTION

Myosin Va, an actin-based motor protein that is conserved from flies to mammals, is expressed in a wide variety of tissues and cell types, with particular enrichment in melanocytes and the brain [Provance and Mercer, 1999; Reck-Peterson et al., 2000; Langford, 2002].

Contract grant sponsor: National Institute of Health; Contract grant number: HD18577; Contract grant sponsor: Evelyn Hart Watson Scholarship.

Robbin D. Eppinga's present address is Center for Basic Research in Digestive Diseases, Department of Biochemistry and Molecular Biology, Mayo Clinic School, Rochester, MN 55905.

I-Feng Peng's present address is Department of Ophthalmology, University of California, San Francisco, San Francisco, CA 94143.

*Correspondence to: Dr. Jim J-.C. Lin, 340 Biology Building East, Department of Biological Sciences, University of Iowa, Iowa City, IA 52242-1324. E-mail: jim-lin@uiowa.edu.

Received 3 April 2007; revised 11 September 2007; Accepted 18 October 2007

Published online 28 November 2007 in Wiley InterScience (www.interscience.wiley.com).
DOI: 10.1002/cm.20255

Mutations in the mouse myosin Va gene, *dilute*, lead to two visible phenotypes, a dilution or lightening of the coat color, and a neurological disorder that is characterized by convulsions and premature death [Searle, 1952] and resembles human Griscelli's disease [Pastural et al., 1997]. An abnormal distribution of perinuclear melanosomes has been found to account for the lightened body color [Provance et al., 1996; Evans et al., 1997; Wu et al., 1997]. The cause of the neurologic defect is still unknown. However, myosin Va associates with a variety of neuronal cargos including neuroendocrine secretory vesicles [Rudolf et al., 2003] and small synaptic vesicles [Prekeris and Terrian, 1997; Evans et al., 1998; Miller and Sheetz, 2000], and it is localized in the postsynaptic density of dendrites [Wang et al., 1996; Walikonis et al., 2000]. Also, myosin Va associates with smooth endoplasmic reticulum (ER) [Tabb et al., 1998], and Purkinje cells that bear substantially reduced myosin Va levels lack smooth ER in their dendritic spines [Dekker-Ohno et al., 1996; Takagishi and Murata, 2006]. These observations have led to a model where myosin Va plays a physiological role in capturing intracellular vesicles/organelles in the actin-rich periphery [Wu et al., 1998a]. In the absence of myosin Va, microtubule-dependent melanosome movement is greatly enhanced in the melanocytes derived from *dilute* mice [Provance et al., 1996; Wei et al., 1997; Wu et al., 1998a]. The organelle movement in the *dilute-lethal* neurites is predominantly in the anterograde direction, and the maximum rates of organelle movements in these neurites are significantly faster than that in the wild type or heterozgous cells [Bridgman, 1999].

In addition to intracellular transport, myosin Va might play a role in regulating the cytoskeleton. Myosin Va interacts with microtubules [Waterman-Storer et al., 2000; Cao et al., 2004], with microtubule-interacting proteins EB1 [Wu et al., 2005], kinesin [Huang et al., 1999], and a dynein light chain [Espindola et al., 2000], as well as with intermediate filaments [Bridgman, 1999; Rao et al., 2002]. Additionally, biochemical studies have shown that myosin Va has the ability to directly assemble actin into anti-parallel bundles [Cheney et al., 1993; Tauhata et al., 2001] and to crosslink tubulin together with actin [Cao et al., 2004], suggesting that myosin Va might be involved in the organization of the actin cytoskeleton in vivo.

Although myosin Va has been implicated in the regulation of cell morphology [Edgar and Bennett, 1999], filopodia motility [Wang et al., 1996], and neurite extension [Takagishi et al., 2007], no clear role in cytoskeleton regulation or cell migration has been described. Here, we address this question in two different cell types. First, we overexpress a GFP-tagged brain isoform of myosin Va (GFP-M5) [Wu et al., 2002] or a C-terminally truncated version (GFP-M5Δ) in CHO cells. GFP-M5 contains an actin-binding motor domain with ATPase activity, a neck domain composed of six consensus IQ motifs that are bound by light chain calmodulin, a PEST site that is recognized by the protease calpain, coiled coil domains that facilitate myosin Va dimerization, and a globular tail domain that can bind a variety of cargos (Fig. 1A). The truncated version, which lacks the globular tail domain but retains the dimerization domain, has previously been shown to form dimers, to bind actin, and to be constitutively active in vitro [Wang et al., 2000]. Second, we analyzed neurons from transgenic *Drosophila* that express mouse M5Δ fused to red fluorescent protein (M5Δ-dsRed) and neurons cultured from a *Drosophila* mutant that bears a nonsense mutation ($MyoV^{Q1052st}$) in the *Drosophila* myosin V, *didum* [Mermall et al., 2005; Li et al., 2007]. We report that overexpression of myosin V and tailless myosin Va results in distinct, often opposite, effects on cell spreading, cell migration, and cytoskeleton architecture, suggesting that supraphysiological levels of either protein has the ability to influence actin cytoskeleton organization and cell motility.

MATERIALS AND METHODS

Plasmids

GFP-tagged full length myosin Va (GFP-M5) cDNA was a generous gift from J.A. Hammer, III (National Institutes of Health, Bethesda, MD) and was previously named GFP-BR MV [Wu et al., 2002]. GFP-tailless myosin Va (GFP-M5Δ) was constructed from plasmids pEGFP-C2 (Clontech, Mountain View, CA), pSpecG (encoding myosin Va nucleotides 41-3311; accession X57377) and pC23 (encoding nucleotides 1549-3928) [Mercer et al., 1991]. pSpecG and pC23 were generous gifts from N.A. Jenkins (National Cancer Institute, Fredrick, MD). pSpecG was digested with ApaI and EcoRI, pC23 was digested with EcoRI and Eco47III, and pEGFP-C2 was digested with BamHI followed by Klenow fill-in and subsequent ApaI digestion. The resulting 1.5, 1.75, and 4.7 kb fragments were isolated and re-ligated to produce pEGFP-M5Δ which encodes GFP fused to the first 1091 amino acids of myosin Va (Fig. 1A).

Plasmids pUAST-DsRed and pUAST-M5Δ-DsRed were constructed from pDsRed-Express-N1 (Clontech) and the Gal4-inducible, white-eye selectable vector pUAST, a generous gift from Wayne Johnson (University of Iowa, Iowa City, IA). To construct pUAST-DsRed, a 703 bp SmaI/NotI digested DsRed fragment from pDsRed-Express-N1 was filled in with Klenow and subcloned into the 9.05 kb Acc65I digested and filled-in site of pUAST. To construct pUAST-M5Δ-DsRed, M5Δ was iso-

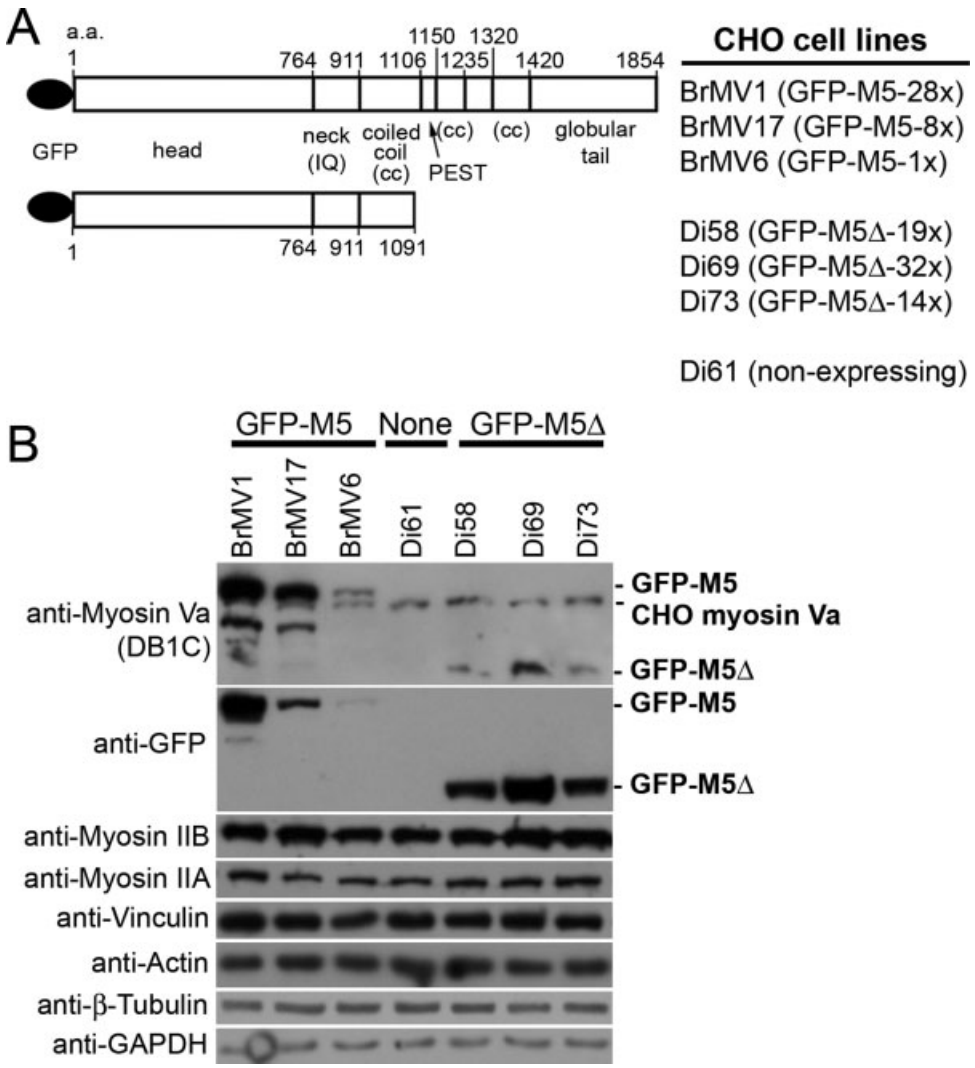

Fig. 1. GFP-M5 and GFP-M5Δ constructs, their stably expressing lines, and their protein expression levels. Cell lines BrMV1 (GFP-M5-28×), BrMV17 (GFP-M5-8×) and BrMV6 (GFP-M5-1×) stably express GFP (black ovals) fused to M5. GFP-M5Δ (retaining the actin-binding head domain, the calmodulin-binding IQ motifs in the neck domain, and the first coiled coil dimerization domain, but lacking the cargo-binding tail domain) was expressed in Di58 (GFP-M5Δ-19×), Di69 (GFP-M5Δ-32×), and Di73 (GFP-M5Δ-14×) cell lines. Concomitantly cloned cell line Di61 expressed no exogenous protein and served as a control line. (**B**) Western analysis on extracts from stable cell lines using the indicated antibodies. Cell lines used in this study express various amounts of GFP-M5 or GFP-M5Δ without affecting the expression levels of endogenous myosin Va, myosin IIB, myosin IIA, vinculin, actin, β-tubulin or GAPDH.

lated from SalI-digested pEGFP-dilute1a-2, a derivative of pEGFP-M5Δ, and ligated into SalI-digested pUAST-DsRed. All plasmids were verified by sequencing.

Cell Culture, Cell Cloning, and Scoring Multinuclearity

CHO cells grown in Dulbecco Modified Eagle's medium (DMEM) plus 10% fetal bovine serum (FBS) were transfected with Lipofectamine (Invitrogen Corp, Grand Island, NY), selected, screened, and cloned as previously described [Warren et al., 1994] to obtain stable expression lines. Growth rate measurements were performed as previously described [Li et al., 2004b]. To score multinuclearity, cells were plated on coverslips, stained at 25°C for 15 min with 10 ng/ml DAPI (4′,6′-diamidino-2-phenylindole; Sigma-Aldrich Co, St Louis, MO), imaged randomly, and scored manually for having three or more nuclei [Warren et al., 1995].

Immunoprecipitation and Western Blot Analyses

Cells from 95% confluent 100-mm dishes were washed and harvested in 1-ml IB buffer (20 mM sodium phosphate buffer pH 7.5, 150 mM NaCl, 1% NP-40, 1 mM ATP, 1 mM $MgCl_2$) supplemented with complete protease inhibitor cocktail (Roche Applied Science, Indianapolis, IN). Cell extracts were centrifuged at 14,000*g* at 4°C for 15 min. The supernatant was preabsorbed for 20 min at 4°C with 10-μg protein A-sepharose beads (Amersham Biosciences, Piscataway, NJ). The clarified and preabsorbed lysates were then incubated with 1-μg anti-GFP polyclonal antibody (Clontech no. 8371-2) for 1 h at 4°C with rotation before adding 10-μg protein A-sepharose and incubating for 1 h at 4°C. After centrifugation, precipitates were washed three times with IB buffer and then dissolved in 2×SDS-PAGE sample buffer. The solubilized proteins were resolved on 7.5% SDS-PAGE gels and subjected to Western blot analysis.

The primary antibodies and dilutions in cell culture medium included: anti-myosin Va DB1C (1:1000) (a generous gift from R.S. Walikonis, University of Connecticut, CT and J.A. Mercer, McLaughlin Research Institute, Great Falls, MT) [Walikonis et al., 2000], anti-DsRed (1:2500) (Clontech), anti-GFP (1:1000) (Clontech), anti-vinculin hVIN-1 (1:2000) (Sigma), anti-actin JLA-20 (1:2000), anti-β-tubulin (1:2000), anti-GAPDH (1:2000) (Sigma), anti-myosin IIA MHC-A (1:500) and anti-myosin IIB MHC-B (1:5000) (Covance Research Products, Berkley, CA) followed by HRP-conjugated secondary antibodies (Sigma) and chemiluminescence detection. ImageJ software (NIH, http://rsb.info.nih.gov/ij/download.html) was used to quantify Western blot band intensities.

Wound Healing, Spreading Assays, and Morphology Analysis

Wound healing assays were performed as described previously [Eppinga et al., 2006b]. Briefly, confluent cell monolayers were wounded with a plastic pipette tip and imaged on a Leica DMIRE2 microscope at 10× magnification every 2 h for 24 h and the decrease in wound width was measured with Openlab software (Improvision Inc., Lexington, MA). Alternatively, cell monolayers were wounded and allowed to recover for 1 h, assembled into a Dvorak-Stotler perfusion chamber (Nicholson Precision Instruments, Inc, Gaithersburg, MD), and digitally recorded on the Zeiss Axiovert (40×) for 4 h at 30 s intervals. Resulting images were traced with 2D-DIAS, 2-Dimensional-Dynamic Image Analysis Software [Soll, 1995; Soll and Voss, 1998], and quantitative morphology and motility parameters were calculated for individual cells.

Cell spreading was determined by plating trypsinized cells on glass, fixing coverslips at 5, 15, 30, 45, 60 min and 48 h, imaging 50 cells at random at 63× magnification, and calculating cell morphology parameters using 2D-DIAS. Roundness is a measure of morphological polarity expressed as a percentage where 100% represents a perfect circle. A decrease in roundness indicates the production of asymmetrically arranged protrusions that contribute to morphological polarity. Mean convexity is a measure of shape complexity where a perfect circle would have 360° convexity. Higher convexity values indicate more or larger protrusions at the cell periphery. Each protrusion, defined as a convex region of membrane flanked by concave regions, adds ~180° to convexity.

Construction of Transgenic Flies and Genetic Crosses

Two plasmids, pUAST-DsRed and pUAST-M5Δ-DsRed, were individually injected into w^{1118} *Drosophila* embryos before cellularization by Genetic Services, Inc (Sudbury, MA). Positive individuals, carrying mini-white (w^+) gene products, were backcrossed to generate stable transgenic lines, and confirmed to express fluorescent DsRed or DsRed-M5Δ in the central nervous system after mating with pan-neuronal driver Gal4 line elav^{c155}-GAL4. Single copies of elav^{c155}-GAL4 and pUAST-DsRed-M5Δ in heterozygotes are sufficient to drive protein expression in embryonic and larval stages. To simultaneously observe two proteins, elav^{c155}-GAL4 flies were crossed with flies carrying pUAST-M5Δ-DsRed together with pUAS-GMA, a UAS-GFP plasmid encoding the F-actin binding domain of moesin [Bloor and Kiehart, 2001]. MyoV^{Q1052st}, a *Drosophila* line produced by EMS mutagenesis encodes a Gln-stop point mutation proximal to the globular tail domain of myosin V [Mermall et al., 2005].

Drosophila "Giant" Neuron Culture and Neurite Outgrowth

Drosophila neurons from single embryos were cultured on uncoated coverslips in medium (80% *Drosophila* Schneider medium and 20% FBS, with 200 ng/ml insulin, 50 μg/ml streptomycin, and 50 U/ml penicillin) as previously described [Saito and Wu, 1991; Yao and Wu, 1999; Yao et al., 2000]. To generate ''giant'' neurons from neuroblasts, cytochalasin B at 2 μg/ml was added during the first 24 h of culture to arrest cytokinesis and was subsequently removed after washing, as described previously [Wu et al., 1990; Peng and Wu, 2007]. To determine neurite growth, individual neurons were located and imaged at 6, 12, 24, 48, and 72 h. The length of neurites was measured with ImageJ software (NIH).

Fluorescence Microscopy

Cells were fixed and permeabilized as described previously [Eppinga et al., 2006a] and were incubated with the following primary antibodies: DB1C (1:100), MHC-A (1:100) MHC-B (1:500), and hVIN-1 (1:500). FITC-conjugated phalloidin (1:200) (Molecular Probes, Inc., Eugene, OR) was used at 37°C for 10 min to visualize F-actin. All fixed cells were mounted to slides with gelvatol [Hegmann et al., 1989] and imaged on a Zeiss Photomicroscope III or Leica DMIRE2 microscope. Images were recorded with a cooled CCD camera (QImaging, Burnaby, BC, Canada) and Openlab software. To observe endocytosed vesicles, CHO cells were labeled for 1 h with 60 μM FM4-64, washed briefly in phosphate buffered saline, and imaged live at 37°C in the presence of growth media using a 63× objective on a Leica DMIRE2 microscope.

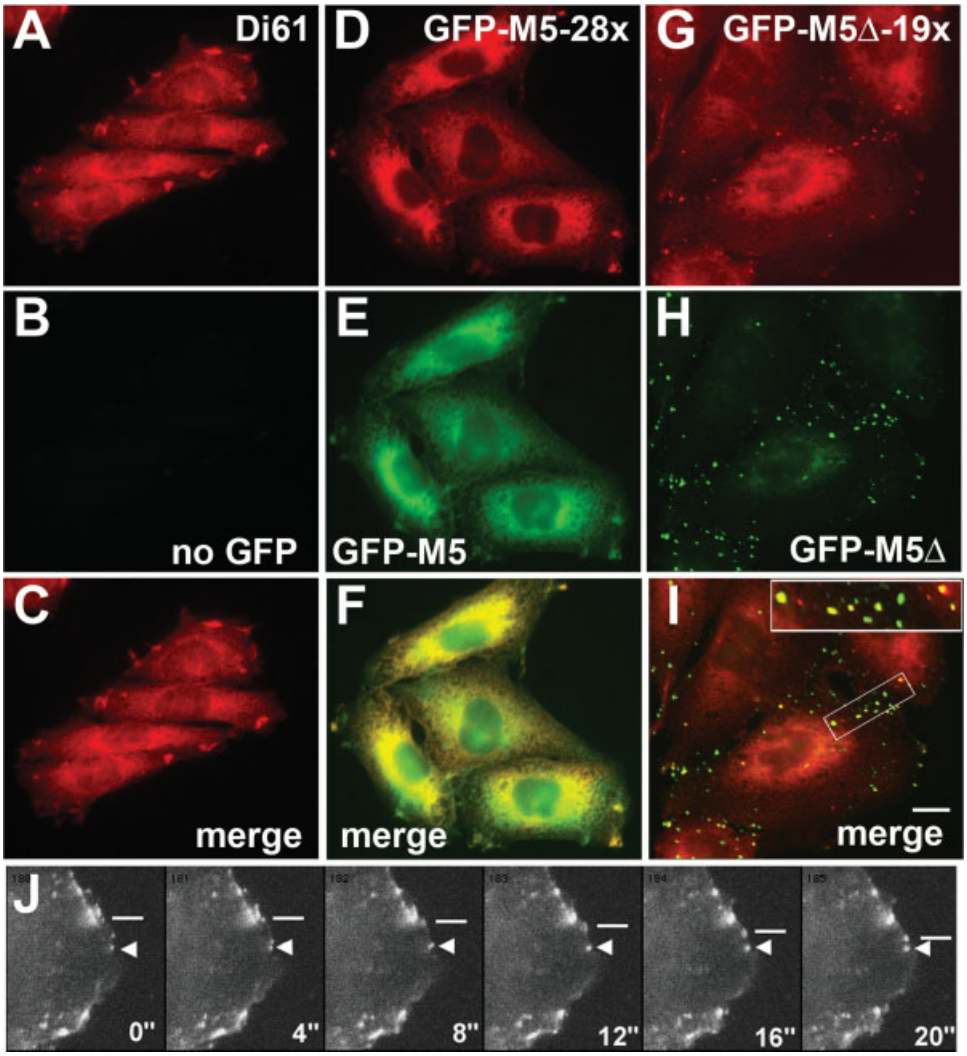

Fig. 2. Subcellular localization of CHO myosin Va, GFP-M5 and GFP-M5Δ. Non-expressing Di61 cells (**A–C**), GFP-M5-28× cells (**D–F**), and GFP-M5Δ-19× cells (**G–I**) were labeled with anti-myosin Va antibody DB1C (A,D,G), imaged for GFP fluorescence (B,E,H), and the images were merged (C,F,I). Before image adjustment, DB1C-fluorescence was stronger in GFP-M5-28× cells and weaker in GFP-M5Δ-19× cells than in Di61 cells. CHO myosin Va and GFP-M5 localized to a patched, tubular network prominent near the nucleus and observable in peripheral ruffles. In GFP-M5Δ-19× cells, GFP-M5Δ was observed in puncta of various size. A subset of the GFP-M5Δ puncta were recognized by anti-myosin Va antibody DB1C (inset in I). Scale bar represents 10 μm. (**J**) A 20 second confocal microscopy time-lapse series of GFP-M5Δ-19× cells shows two small puncta (bars) that migrate individually from one collection of puncta toward another punctum (arrowhead), revealing that puncta are mobile, not stable aggregates.

RESULTS

GFP-M5 and GFP-M5Δ Expression in Stable CHO Cell Lines

Clonal cell lines that express various amounts of GFP-M5 or GFP-M5Δ, were isolated and expression levels were determined by Western blot (Fig. 1). Cell lines BrMV1, BrMV17, and BrMV6 express ∼28, 8, and 1 times, respectively, the amount of GFP-M5 as endogenous CHO myosin Va, as detected by the polyclonal anti-myosin Va antibody DB1C. The DB1C antibody recognized GFP-M5 and a degradation product that was less apparent with the GFP antibody. DB1C was generated against the coiled coil and tail portion (amino acids 1042–1854) of myosin Va [Walikonis et al., 2000] and reacts poorly with GFP-M5Δ. To estimate relative GFP-M5Δ expression levels, a monoclonal anti-GFP antibody was used. Stable lines Di58, Di69, and Di73 express ∼19, 32, and 14 times as much GFP-M5Δ as endogenous myosin Va. Di61, a drug resistant line isolated during the cloning procedure, expresses no GFP-fusion protein and was used as a control cell line for further experiments. Expression of either GFP-M5 or GFP-M5Δ had no substantial effect on the protein level of endogenous myosin Va nor on the levels of cytoskeleton proteins myosin IIB, myosin IIA, vinculin, actin, or tubulin, compared to GAPDH (Fig. 1B). For a convenience to follow the expressed protein and expression level for the various cell lines, the nomenclatures by construct and fold expression were adopted, for examples, BrMV1 = GFP-M5-28×, Di58 = GFP-M5Δ-19×, Di61 = non-expressing, etc (Fig. 1A).

Consistent with previous reports on myosin Va subcellular localization, [Espreafico et al., 1992; Nascimento et al., 1997; Lionne et al., 2001], CHO myosin Va and overexpressed GFP-M5 accumulate to a patched, tubular network, enriched near the nucleus and to protrusions in the cell periphery (Figs. 2A–2F). In contrast, GFP-M5Δ accumulates as distinct puncta of various

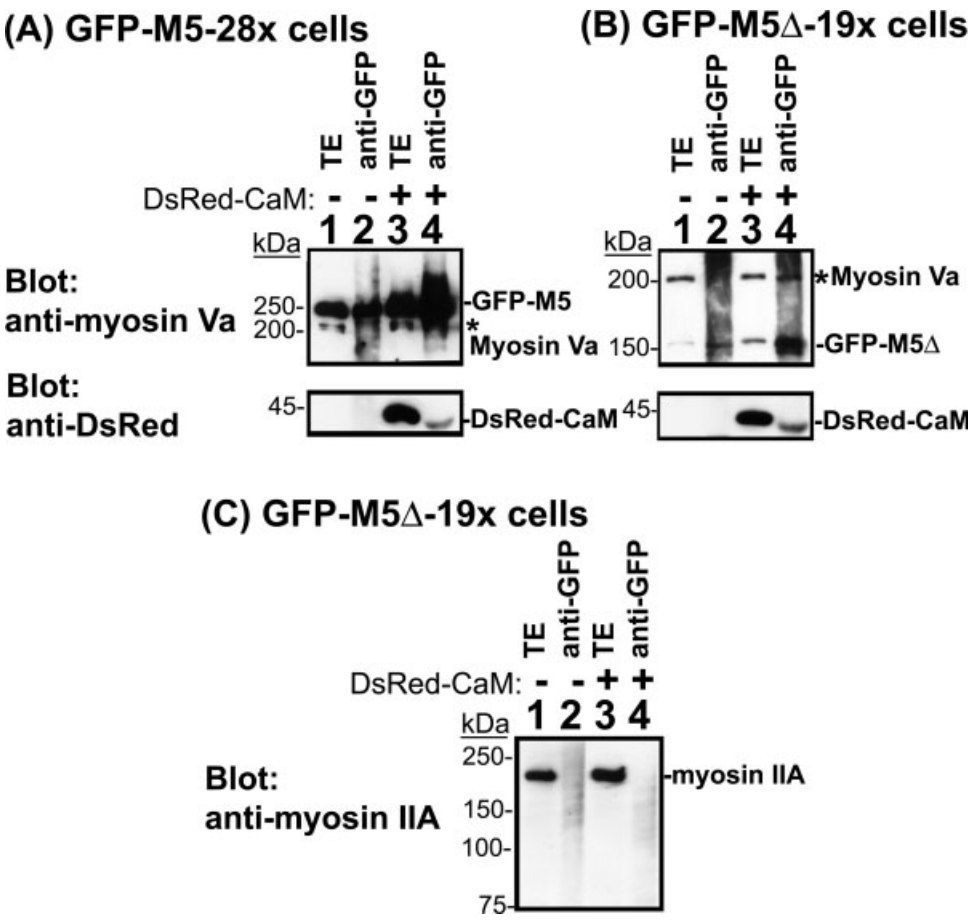

Fig. 3. GFP-M5 and GFP-M5Δ co-immunoprecipitate with CHO myosin Va but not CHO myosin IIA. Total extracts (TE) or immunoprecipitates (anti-GFP) from GFP-M5-28× cells (**A**) or GFP-M5Δ-19× cells (**B** and **C**) in the absence or presence of transfected DsRed-tagged calmodulin (DsRed-CaM), were immunoblotted with antibodies directed against myosin Va (DB1C) (A and B, top panels), DsRed (A and B, bottom panels) or myosin IIA (C). 200 kDa CHO myosin Va (asterisk in A and B) was detectable in precipitates in the absence (A and B, lane 2), and more so in the presence (A and B, lane 4), of exogenous calmodulin expression. Notably, myosin IIA was absent in the anti-GFP immunoprecipitates from GFP-M5Δ-19× cells, regardless of the presence of DsRed-CaM expression.

sizes that are distributed throughout the CHO cell body with particularly large puncta accumulating at the cell edges (Figs. 2G–2I). Anti-myosin Va antibody (DB1C) recognized a subset of the GFP-M5Δ puncta (Fig. 2I, inset). Time-lapse imaging revealed that GFP-M5Δ puncta are dynamic collections of smaller puncta. Puncta within these collections can migrate individually from one region of accumulation to a second region (Fig. 2J) or can disperse rapidly.

GFP-M5 and GFP-M5Δ Immunoprecipitate With Endogenous CHO Myosin Va

Because both GFP-M5 and GFP-M5Δ retain the dimerization domain, it was possible that they could dimerize with endogenous myosin Va. To investigate this, we used a GFP antibody to immunoprecipitate the GFP-fusion proteins from cell extracts in the absence and presence of the co-expressed red fluorescent protein fused to calmodulin (DsRed-CaM). Anti-myosin Va antibody (DB1C) detected endogenous myosin Va (asterisk in Fig. 3A) and GFP-M5 in immunoprecipitates from GFP-M5-28× cells in the absence of DsRed-CaM (lane 2). The association was more apparent in the presence of DsRed-CaM expression (lane 4). Similarly, endogenous myosin Va (asterisk in Fig. 3B) co-immunoprecipitated with GFP-M5Δ from GFP-M5Δ-19× cells (lane 2) and again, this interaction was increased in the presence of DsRed-CaM (lanes 4). In contrast, myosin IIA did not co-immunoprecipitate with GFP-M5Δ and myosin IIA protein levels were not affected by DsRed-CaM expression (Fig. 3C). These data suggest that force-expressed GFP-M5 and GFP-M5Δ associate with CHO myosin Va in vivo.

Expression of GFP-M5Δ Slows Cell Growth Rate and Alters Cell Shape

To examine whether GFP-M5Δ expression affects CHO cell division, the population doubling time and percent of multinucleate cells were determined for GFP-M5Δ expressing lines. Similar to wild type CHO cells [Warren et al., 1994; Li et al., 2004b], non-expressing Di61 cells double every 19 h and exhibit a basal level (8.5%) of multinucleate cells (Table I). In contrast, all GFP-M5Δ-expressing cell lines showed

TABLE I. Division Time, Percent Multinucleate, and Interphase Morphology Characterization on CHO Cell Lines Expressing GFP-M5Δ

Cell line	Division time (h)	Cell number	Cells with >2 nuclei (%)	Cell number	Area (μm^2) mean ± S.E.M.	Roundness (%) mean ± S.E.M.
Di61[a]	19	1039	8.5	252	453.7 ± 19.7	34.5 ± 0.8
Di73 (GFP-M5Δ-14×)[b]	26	1016	**34.6**	268	**535.0 ± 20.1**	**53.1 ± 0.9**
Di69 (GFP-M5Δ-32×)[c]	25	1009	**32.3**	262	**602 ± 21.0**	**52.9 ± 0.9**
Di58 (GFP-M5Δ-19×)[d]	27	1005	**34.5**	214	**662 ± 28.5**	**48.0 ± 1.0**
P value		(a vs. b)*	**<0.001**	(a vs. b)**	**0.0013**	**<0.0001**
		(a vs. c)*	**<0.001**	(a vs. c)**	**<0.0001**	**<0.0001**
		(a vs. d)*	**<0.001**	(a vs. d)**	**<0.0001**	**<0.0001**

For statistics, Sigma Stat software was used to perform a *z* test (*) or a *T* test (**). If normality or equal variance tests failed in a *T* test, Rank-Sum analyses were performed. Bold numbers are significant.

increased doubling time and an increased incidence of multinucleate cells. Similar observations have been made for melanocytes lacking myosin Va [Provance et al., 1996; Wu et al., 1998b]. These data are consistent with idea that GFP-M5Δ inhibits endogenous myosin Va function.

To investigate whether GFP-M5Δ expression affects cell shape, we analyzed interphase cells that were cultured for 48 h. Cells from all GFP-M5Δ-expressing lines were, on average, larger and more round than non-expressing Di61 cells (Table I). However, the GFP-M5-28× cell line was also larger (676 ± 20 μm^2) and more round (58.2% ± 0.8%) than non-expressing Di61 cells (453.7 ± 19.7 μm^2, $P < 0.001$; 34.5% ± 0.8%, $P < 0.001$). Therefore, expression of either GFP-M5Δ or GFP-M5 causes an increase in cell area and a decrease in morphological polarity.

GFP-M5 and GFP-M5Δ Expression Alters the Distribution of Vesicles Oppositely

Since myosin Va activity has been reported to influence the distribution and migration of intracellular vesicles, we investigated whether GFP-M5 or GFP-M5Δ affect the distribution of endocytosed FM4-64, a lipophilic dye. Endocytic vesicle-like FM4-64 puncta were observed throughout control Di61cells, with occasional enrichment near the cell center or at the tips of cells (Fig. 4A). FM4-64 puncta accumulated to discontinuous patches near the cell tips of GFP-M5-28× cells and were mostly absent from the center (Fig. 4B). In contrast, FM4-64 puncta were enriched near the cell center of GFP-M5Δ-19× cells in large aggregations (Figs. 4C and 4D), reminiscent of melanosome distribution in melanocytes that lack myosin Va [Wei et al., 1997]. GFP-M5Δ puncta did not colocalize with FM4-64 puncta (Figs. 4D and 4E), suggesting that the centralized localization of FM4-64 puncta is an indirect effect of GFP-M5Δ expression. These data are consistent with a role for myosin Va in promoting peripheral vesicle accumulation.

Cell Spreading Dynamics are Altered by GFP-M5 and GFP-M5Δ Expression

We next investigated whether expression of GFP-M5 or GFP-M5Δ alters the dynamics of cell spreading. Although control Di61 cells, GFP-M5-28× cells, and GFP-M5Δ-19× cells were able to spread (indicated by increased area with time), to elongate (indicated by decreased roundness), and to produce protrusions (indicated by increased convexity) ($P < 0.001$ for all, Two-Way-ANOVA, Holm-Sidak post hoc test), they did so with different dynamics (Fig. 5). Di61 cells exhibit a progressive increase in area that, for the first 30 min after plating, is coupled with a considerable decrease in roundness, and an increase in convexity. This suggests that non-expressing cells produce asymmetric protrusions to accomplish progressive spreading. GFP-M5Δ-19× cells spread with the same dynamics as Di61 cells for the first 30 min ($P > 0.05$). After 45 min, the rate of elongation (roundness) is reduced ($P < 0.05$) and protrusion formation (convexity) is slowed ($P < 0.05$). GFP-M5-28× cells spread significantly slower than Di61 or GFP-M5Δ-19× cells ($P < 0.05$), are more round ($P < 0.05$ at 30 and 60 min; not different than GFP-M5Δ-19× cells at 45 min), and are less convex ($P < 0.05$). Taken together, these data indicate that GFP-M5 expression inhibits the formation of asymmetric protrusions during cell spreading. GFP-M5Δ expression does not slow the rate of cell spreading but reduces the extent to which cells elongate.

GFP-M5Δ Expression Slows Wound-Edge Migration

To assess the ability of non-expressing Di61, GFP-M5-28×, and GFP-M5Δ-19× cells to migrate, we monitored wound closure over a 24-h period (Fig. 6A).

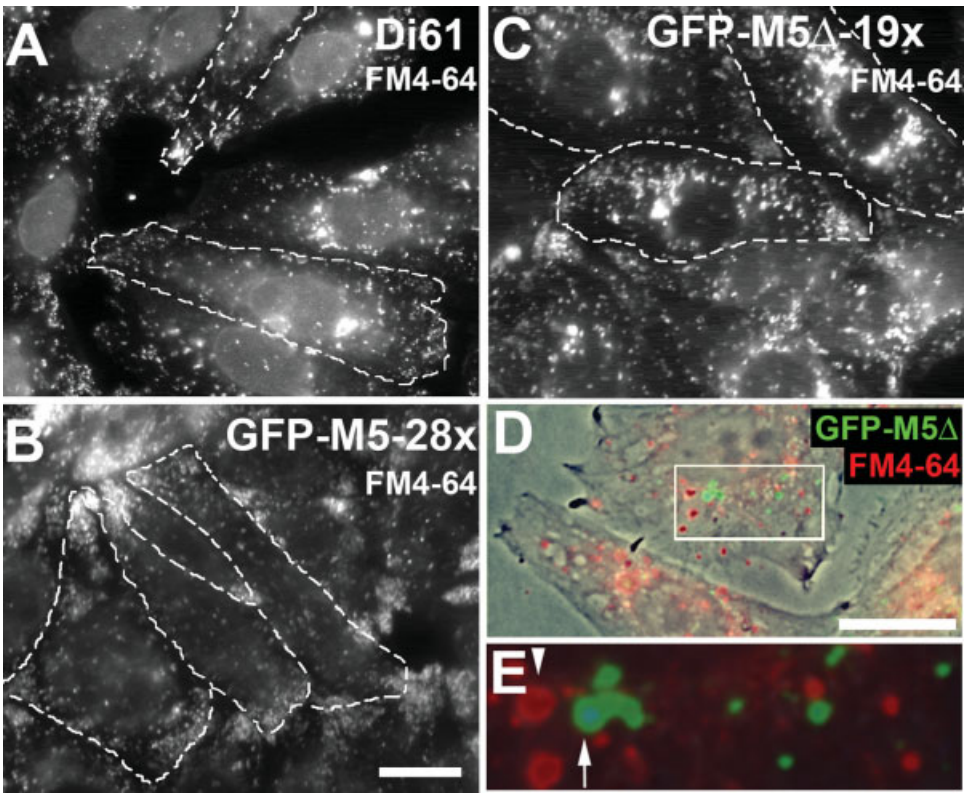

Fig. 4. Endocytosed FM4-64-labeled vesicles collect to the periphery of GFP-M5-expressing cells and near the nucleus of GFP-M5Δ-expressing cells. Non-expressing Di61 cells (**A**), GFP-M5-28× cells (**B**), and GFP-M5Δ-19× cells (**C–E**) were loaded with the marker FM4-64 (white puncta in A–C, red in D–E). FM4-64-labeled vesicles localize throughout Di61 cells with some accumulation near the nucleus or to the cell edge (A). In contrast, vesicles collect at the periphery of GFP-M5-28× cells (B) and near the nucleus in GFP-M5Δ-19× cells (C). (D-E) Images of GFP-M5Δ puncta (green) and FM4-64-labeled vesicles (red) in GFP-M5Δ-19× cells were merged with (D) or without (E) the phase image to show that although GFP-M5Δ puncta (arrow in E) localize near vesicles (arrowhead in E), the two types of puncta are not coincident, suggesting that the altered vesicle distribution is not caused by direct GFP-M5Δ association. Scale bars represent 10 μm.

Di61 monolayers healed progressively. The wound edge migrated at a mean instantaneous speed of 240 nm/min. No statistical difference was observed in wound closure in GFP-M5-28× cells, compared to Di61 cells. In contrast, wound closure in GFP-M5Δ-19× cells was slower than in Di61 or GFP-M5-28× cells ($P < 0.001$ for both) (Fig. 6B). Further, wound closure in GFP-M5Δ-19× cells was slower during the initial 0–8 h than during hours 8–14 ($P < 0.001$), suggesting the presence of a polarization defect as well as a migration defect. These data indicate that GFP-M5Δ expression, but not GFP-M5 expression, slows the progression of wound closure.

GFP-M5Δ Expression Slows Cell Migration and Reduces Lamellipodia Dynamics

Because delayed wound closure in the previous assay could result from defects in migration, in cell polarization and/or in slow proliferation, we examined individual migrating cells that were pre-aligned toward the wound. Non-expressing Di61 cells showed persistent migration toward the wound at a mean instantaneous speed of 191 nm/min (Table II), consistent with monolayer migration between 0 and 8 h (Fig. 6B). Migration dynamics of GFP-M5-1× and GFP-M5-28× cells were the same as Di61 cells (Table II). In contrast, GFP-M5Δ-14×, GFP-M5Δ-32× and GFP-M5Δ-19× cells were slower, less persistent, and migrate less than half the net distance of Di61 cells in the 4-h assay. Reduced net distance is reflected in GFP-M5Δ-19× cell pathfiles as a smaller distance between the initial and final cell centroids (Fig. 7). Lamellipodial expansion (positive flow) and retraction (negative flow) were also reduced in cells expressing GFP-M5Δ, but were normal in cells expressing GFP-M5 (Table II). These data are consistent with a previously reported myosin Va role in filopodial extension [Wang et al., 1996]. Together, the motility

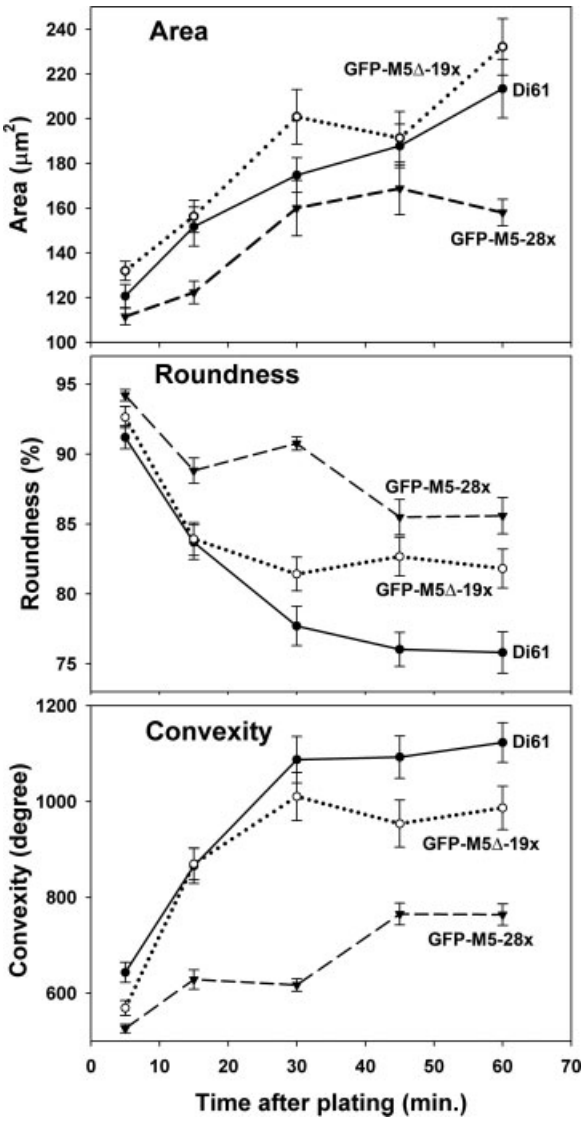

Fig. 5. Expression of GFP-M5 or GFP-M5Δ produces distinct abnormalities during cell spreading. 50 randomly chosen cells from non-expressing Di61cells, GFP-M5-28× cells, and GFP-M5Δ-19× cells were plated on glass coverslips, fixed at 5, 15, 30, 45, and 60 min, and imaged for shape and size analysis. The average area, roundness, and convexity are shown. GFP-M5-28× cells spread more slowly, and GFP-M5Δ-19× cells spread at the same rate as Di61 cells (**A**). GFP-M5-28× and GFP-M5Δ-19× cells were more round/less polarized than control cells (**B**). GFP-M5Δ-19× cells showed reduced, and GFP-M5-28× cells further reduced, convexity, a measure of cell protrusions (**C**). Error bars represent s.e.m.

assays indicated that GFP-M5Δ expression slows migration and lamellipodial dynamics without slowing spreading while GFP-M5 slows spreading without slowing migration. This dichotomous phenotype has been observed after myosin II inactivation [Wylie et al., 1998; Wakatsuki et al., 2003; Lo et al., 2004; Cai et al., 2006], suggesting a possible defect in the actin-myosin II cytoskeleton.

Actin Stress Fibers and Myosin II Bundles are Less Robust in Subconfluent GFP-M5Δ-Expressing Cells and More Robust in GFP-M5-Expressing Cells During Interphase

To investigate whether GFP-M5 or GFP-M5Δ expression alters cytoskeleton organization, interphase cells were stained for actin and myosin II (Fig. 8). Repeatedly, FITC-phalloidin fluorescence was stronger in GFP-M5-28× cells and weaker in GFP-M5Δ-19× cells, than in non-expressing Di61 control cells (insets in Fig. 8 were taken at the same exposure), even though total cellular actin was comparable between lines (Fig. 1B). Additionally, actin stress fiber organization differed between all three cell lines. Peripheral actin bundles were robust in Di61 and GFP-M5-28× cells. However, interior actin bundles (arrowheads in Fig. 8D) appeared thicker and more prominent in GFP-M5-28× cells. In contrast, GFP-M5Δ-19× cells had thin interior actin fibers (arrowheads in Fig. 8G) and few robust peripheral fibers. In addition, peripheral fibers that were oriented towards the cell center were often bent and appeared to terminate prematurely (double-arrows in Fig. 8G).

In all cell lines, myosin IIB stained as speckles that appeared as solid bundles when enriched along an actin fiber. Like actin bundles, myosin IIB bundles were prominent near the cell edge of Di61 and GFP-M5-28× cells (arrows in Figs. 8B and 8E; merged in 8C and 8F) and were more robust in the interior of GFP-M5-28× cells. In contrast, few solid bundles were observed in GFP-M5Δ-19× cells. Instead, myosin IIB speckles were more evenly distributed within the cell, accumulating in regions that were coincident with the thin actin stress fibers (Figs. 8H and 8I). The same result was observed when cells were co-labeled for actin and myosin IIA except that myosin IIA exhibited preferential localization nearer to the cell edge and was mostly absent from the robust internal actin bundles in GFP-M5-28× cells [Eppinga and Lin, unpublished]. These data indicate that GFP-M5 expression promotes internal actin and myosin II bundles in interphase cells while GFP-M5Δ expression leads to the opposite phenotype.

Actin Stress Fibers, Myosin II Bundles and Focal Adhesions are Disorganized in Migrating GFP-M5Δ CHO Cells

To determine whether stress fibers were also affected during cell migration, wounded monolayers were stained for actin cytoskeleton markers. Similar to interphase cells, migrating GFP-M5-28× cells showed

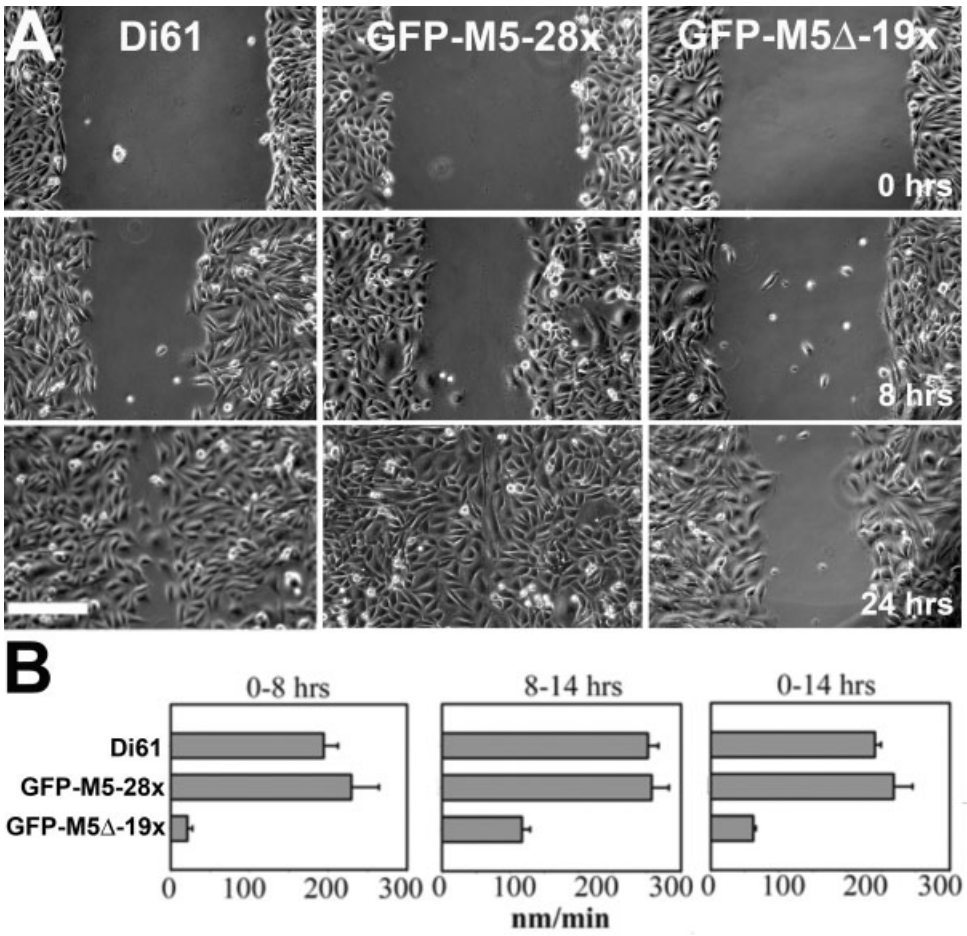

Fig. 6. GFP-M5Δ expression slows wound healing. (**A**) Non-expressing Di61 cells, GFP-M5-28× cells, or GFP-M5Δ-19× cells were plated to confluence and wounded with a plastic pipette. Wound closure was monitored over a 24-h period by imaging wounds every 2 h and measuring the wound width. (**B**) The rate of wound closure reveals that GFP-M5Δ-19× cells closed wounds significantly slower than Di61 or GFP-M5-28× cells. Scale bar represents 150 μm.

TABLE II. Migration of Nonexpressing, GFP-M5-Expressing, and GFP-M5Δ-Expressing CHO Cells During Wound Healing

Cell line	Cell number	Instantaneous speed (nm/min)	Persistence (nm/min-degree)	Total distance (μm)	Net distance (μm)	Positive flow (%)	Negative flow (%)
Di61[a]	11	191 ± 9	37.0 ± 4.1	74.9 ± 3.6	21.6 ± 2.8	9.1 ± 0.5	8.5 ± 0.5
BrMV6 (GFP-M5-1×)[b]	7	176 ± 13	31.7 ± 5.0	71.5 ± 6.0	15.4 ± 3.4	9.4 ± 0.8	8.6 ± 0.8
BrMV1 (GFP-M5-28×)[c]	14	174 ± 8	27.5 ± 2.9	76.2 ± 3.9	15.9 ± 1.5	9.1 ± 0.7	8.0 ± 0.6
Di73 (GFP-M5Δ-14×)[d]	13	**141 ± 6**	**21.9 ± 2.0**	**57.2 ± 2.9**	10.7 ± 1.2	**6.9 ± 0.3**	**5.8 ± 0.30**
Di69 (GFP-M5Δ-32×)[e]	15	**135 ± 4**	**20.4 ± 1.2**	**53.6 ± 1.9**	**7.9 ± 0.7**	7.5 ± 0.4	**6.5 ± 0.3**
Di58 (GFP-M5Δ-19x)[f]	16	**147 ± 9**	**22.8 ± 2.7**	61.7 ± 3.6	**9.4 ± 1.8**	**5.9 ± 0.4**	**5.7 ± 0.4**
P value	(a vs. b)	NS	NS	NS	NS	NS	NS
	(a vs. c)	NS	NS	NS	NS	NS	NS
	(a vs. d)	**<0.05**	**<0.05**	**<0.05**	NS	**<0.05**	**<0.05**
	(a vs. e)	**<0.05**	**<0.05**	**<0.05**	**<0.05**	NS	**<0.05**
	(a vs. f)	**<0.05**	**<0.05**	NS	**<0.05**	**<0.05**	**<0.05**

Cell centroids were tracked for 4.5 h with a 5 min frame rate. Data are shown as mean ± S.E.M. For statistics, Sigma Stat software was used to perform a One Way ANOVA followed by a Holm–Sidak pairwise comparison (if tests of normality and equal variance passed) or by Dunn's method (if normality or equal variance tests failed). NS = not significant, $P > 0.05$.

stronger overall FITC-phalloidin fluorescence and GFP-M5Δ-19× cells showed weaker fluorescence, compared to non-expressing Di61 cells (data not shown). Further, actin bundle organization differed between lines (Fig. 9). Di61 and GFP-M5-28× cells had distinct peripheral actin fibers that were coincident with myosin IIB bundles. Internal actin and myosin bundles were more apparent in GFP-M5-28× cells. In contrast, actin fibers in migrating GFP-M5Δ-19× cells were thinner, mostly confined to the lateral periphery or to transverse fibers behind the lamellipodia, and were truncated and bent when oriented toward the cell center. The myosin IIB

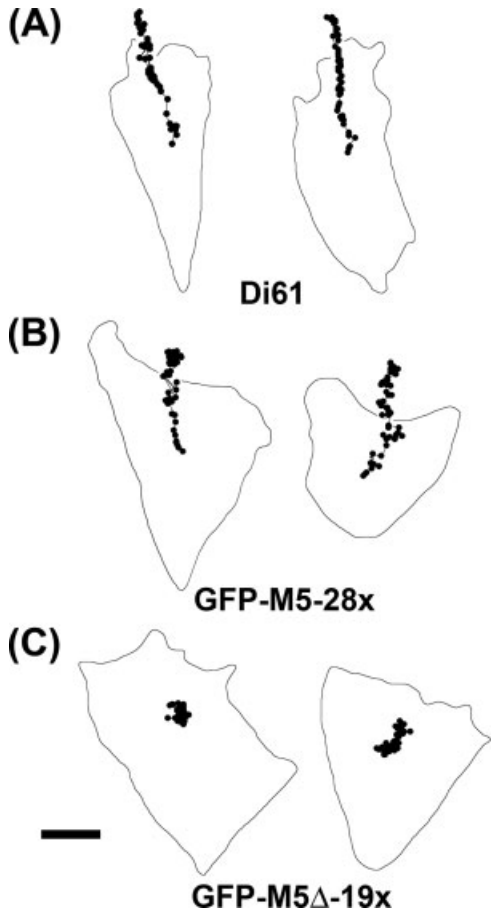

Fig. 7. GFP-M5Δ expression slows cell migration and reduces lamellipodia dynamics. Migrating Di61 cells (**A**), GFP-M5-28× cells (**B**), and GFP-M5Δ-19× cells (**C**) were tracked for 4.5 h. Cells that were best aligned perpendicular to the wound were selected for analysis. Shown are the cell outline at the beginning of analysis, and cell centroid tracks representing the center of cell area at 5 min intervals. Persistent, directional Di61 movement over time is represented by linear tracks and well-spaced centroids. In comparison, GFP-M5-28× cell tracks progress toward the wound but are more tortuous and clustered, reflecting reduced persistence. GFP-M5Δ-19× cells exhibit severely reduced net and total translocation with time, reflected by bunched centroid tracks. Net distance is calculated by the distance between the first and last centroid. Total distance represents the sums of distance between all centroids. The scale bar represents 10 μm.

signal was distributed diffusely through GFP-M5Δ-19× cells, with few solid bundles visible.

Since actin stress fibers are anchored in focal adhesions, we stained migrating cells for vinculin (Fig. 10). Di61 and GFP-M5-28× cells produced peripheral and internal focal adhesions, straight actin stress fibers, and the ends of each fiber coincided with a focal adhesion. Internal focal adhesions were more apparent in GFP-M5-28× cells and were located at the ends of the internal actin bundles. In contrast, GFP-M5Δ-19× cells lacked internal focal adhesions (Fig. 10K). Peripheral actin fibers were anchored by two peripheral focal adhesions or, when extended toward the cell interior, were not anchored internally (Fig. 10L). Together, these data show that GFP-M5 expression leads to more robust internal actin bundles, myosin II bundles, and focal adhesions during cell migration. On the other hand, GFP-M5Δ expression leads to a reduction or complete loss of these internal structures.

Drosophila Neurites Expressing Mouse-Derived Heavy Meromyosin Va or Lacking Functional Endogenous Myosin V Exhibit Reduced Outgrowth

To determine whether the aberrant motility by M5Δ expression were applicable to neuronal cell types, we generated transgenic *Drosophila melanogaster* lines that carry a Gal4-inducible plasmid encoding a fusion between mouse M5Δ and DsRed or a control plasmid encoding DsRed alone (Fig. 11) and crossed these lines to flies expressing pan-neuronal Gal4. The M5Δ-DsRed fusion protein localizes to mobile puncta throughout the soma, neurites, and growth cones of cultured *Drosophila* neurons (Fig. 11B). Neurons cultured from M5Δ-DsRed-expressing fly embryos formed neurites that were morphologically indistinguishable from those of DsRed-expressing controls during the first 12 h in culture. After 12 h, neurites in M5Δ-DsRed-expressing neurons were significantly shorter than neurites in neurons expressing DsRed ($P < 0.0001$, $N = 80$) and remained shorter throughout the 4-day observation period (Figs. 11C and 11D).

To determine whether neurite outgrowth defects resulted from the expression of tailless mouse myosin Va, we analyzed the outgrowth of neurons cultured from flies that bear a nonsense Gln 1052 mutation (Q1052st) in the first coiled coil domain of the sole *Drosophila* myosin V gene, *didum* [Mermall et al., 2005]. Polyclonal antiserum generated against a peptide corresponding to the tail of myosin V detected myosin V in extracts from *Drosophila* heads but detected no full length myosin V from $MyoV^{Q1052st}$ flies [Mermall et al., 2005]. Similar to the transgenic cells, maximal neurite extension was significantly reduced in $MyoV^{Q1052st}$ neurons compared to neurons expressing DsRed ($P = 0.0009$, $N = 313$) (Fig. 11D). Together, these data show that the expression of tailless mouse myosin Va or the absence of functional endogenous myosin V causes neurite elongation defects in neurons.

Actin Stress Fibers are Less Robust in M5Δ-DsRed *Drosophila* Neurons

To investigate whether M5Δ alters actin arrangement in *Drosophila* neurons, flies expressing M5Δ-DsRed were crossed with flies encoding GMA, a fusion

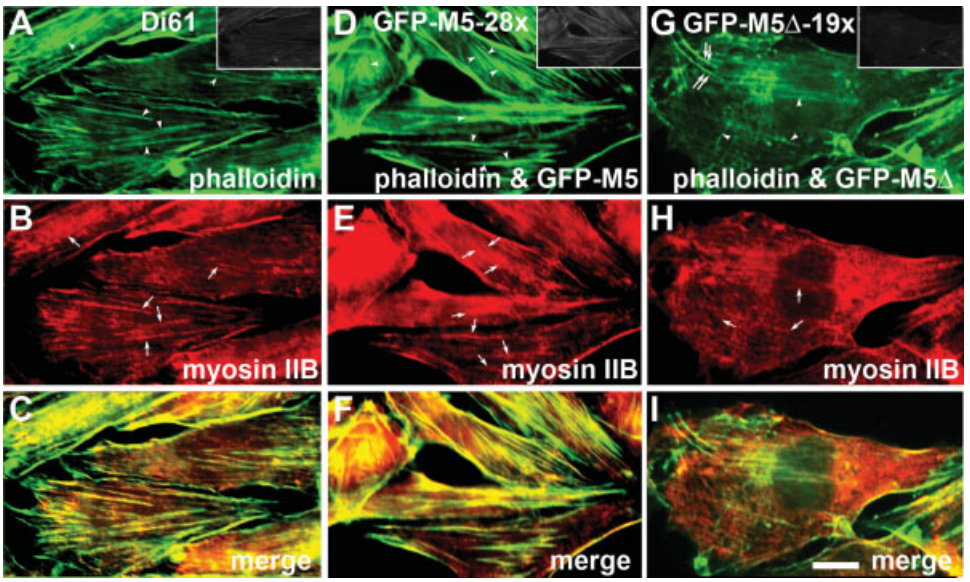

Figure 8.

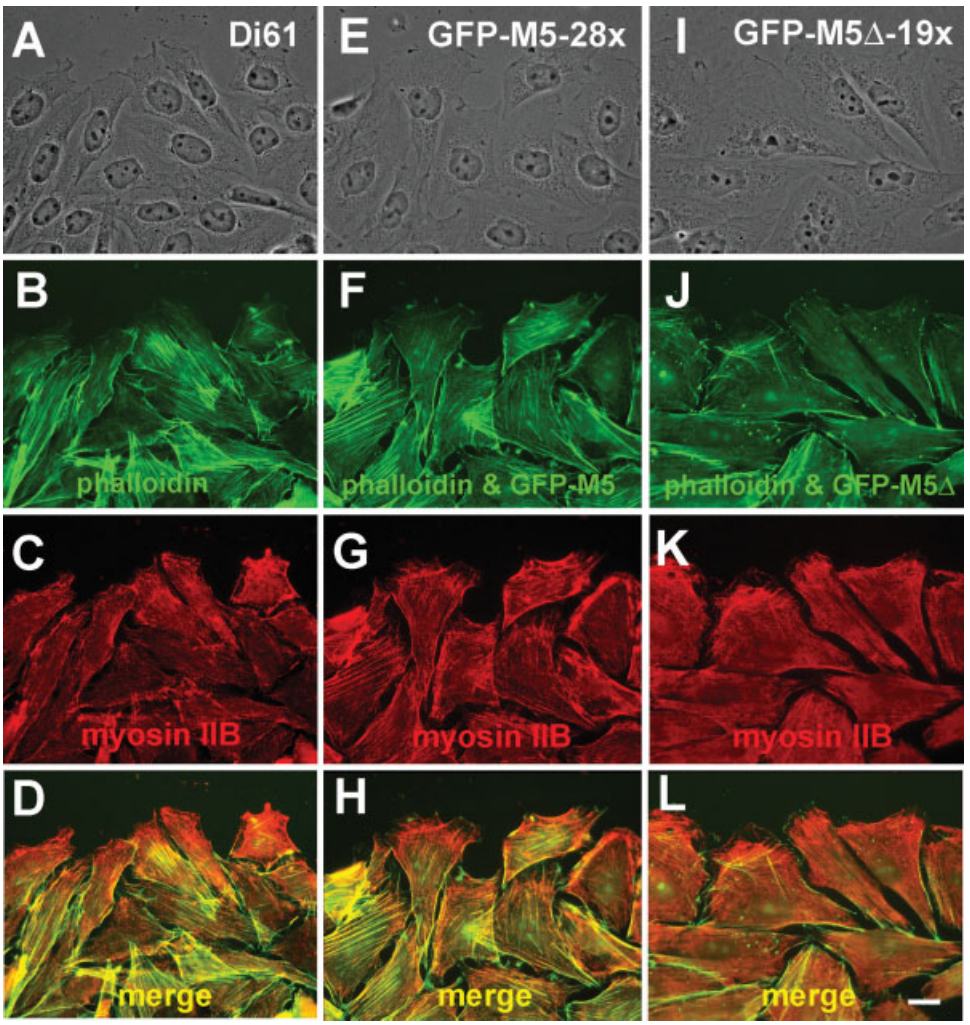

Figure 9.

between GFP and the F-actin binding domain of the *Drosophila* moesin [Edwards et al., 1997; Bloor and Kiehart, 2001; Dutta et al., 2002]. GMA and rhodamine-phalloidin give quantitatively similar labeling of F-actin in *Drosophila* neurons [Andersen et al., 2005]. GMA fluorescence is apparent within the soma and neurites of cultured *Drosophila* neurons in the absence of M5Δ-DsRed (Fig. 12C; cell on left) and the intensity is reduced in co-cultured neurons that express both GMA and M5Δ-DsRed (Fig. 12C; cell on right). Furthermore, fiber-like clusters of GMA are more apparent in the neurites of cells lacking M5Δ-DsRed than in cells expressing M5Δ-DsRed (Fig. 12D). In contrast, MyoV^{Q1052st} neurons stained with phalloidin do not exhibit significant differences in phalloidin intensity or actin organization compared to Canton S controls. Therefore, similar to what was observed in CHO cells, expression of M5Δ-DsRed results in less intensely stained, less organized filamentous actin. However, this phenotype was not mimicked in the absence of functional *Drosophila* myosin V.

DISCUSSION

The observation that overexpressed full length myosin Va enhances actin and myosin bundles is consistent with the known properties of myosin Va. Myosin Va is high duty ratio motor that binds tightly to actin in either an open, active ATPase conformation or a closed, inactive ATPase conformation [Krementsov et al., 2004; Li et al., 2004a; Wang et al., 2004; Liu et al., 2006]. In vitro, myosin Va bundles actin in the presence of ADP or in the presence of ATP with micromolar calcium [Cheney et al., 1993; Tauhata et al., 2001]. Therefore, overexpressed myosin Va could increase actin bundling by crosslinking actin filaments in vivo. Alternatively, myosin Va could induce actin bundling by crosslinking actin and microtubules. Myosin Va associates directly and indirectly with microtubules and crosslinks actin filaments with microtubules in vitro [Huang et al., 1999; Waterman-Storer et al., 2000; Cao et al., 2004; Wu et al., 2005]. Consistent with this, we have observed the greatest gain in actin bundles in the perinuclear region of GFP-M5-28× cells, a region where myosin Va and microtubules are enriched [Wu et al., 1998b].

Although myosin Va overexpression enhances actin bundles, myosin Va is not essential for actin bundle formation. Superior cervical ganglion (SCG) neurons [Evans et al., 1997] and melanocytes [Wei et al., 1997] that were cultured from the *dilute lethal* (null) mice retain actin bundles. The same observation has been made in *Drosophila* MyoV^{Q1052st} mutant where the loss of functional myosin V results in no gross actin cytoskeleton defects and greater than 90% of homozygous progeny die during the 3rd instar larval stage [Mermall et al., 2005]. However, escaper flies develop into viable adults that exhibit subtle actin defects including the malformation of actin-rich investment cones during sperm individualization and ectopic placement of actin-rich rhabdomeres during photoreceptor development [Mermall et al., 2005; Li et al., 2007]. In both cases, the actin defects have been correlated with vesicle trafficking defects, suggesting that myosin V might traffic cargos involved in actin bundle stability. We have observed no difference in phalloidin staining patterns in neurons cultured from MyoV^{Q1052st} and control flies (data not shown), consistent with the non-essential role for myosin V in actin bundle formation.

The mechanism of M5Δ action on the actin cytoskeleton is less clear. The broad array of effects induced by the expression of M5Δ can be explained by one or more of at least three possibilities: (1) M5Δ is out-competing the endogenous myosin Va for cellular targets such as filamentous actin or a cellular protein (e.g.

Fig. 8. GFP-M5 expression enhances and GFP-M5Δ expression reduces actin and myosin IIB bundle organization in CHO cells. Unstimulated, interphase Di61 cells (**A–C**), GFP-M5-28× cells (**D–F**), and GFP-M5Δ-19× cells (**G–I**) were stained with FITC-phalloidin (A,D,G) and anti-myosin IIB (B,E,H). Images taken at the same exposure time (insets in A,C,E) showed that FITC-phalloidin staining was stronger in GFP-M5-28× cells and weaker in GFP-M5Δ-19× cells than in control Di61 cells. Images adjusted to reveal actin organization show that internal actin bundles (arrowheads) are more prominent in GFP-M5-28× cells (D vs. A) and less prominent in GFP-M5Δ-19× cells (G vs. A). Straight peripheral bundles were observed in Di61 and GFP-M5-28× cells, while peripheral bundles in GFP-M5Δ-19× cells were often bent (double arrows in E). Myosin IIB bundles (arrows in B,E,H) were more robust in GFP-M5-28× cells (E) than in control Di61 cells (B) and overlap with actin bundles (C,F, merged). Myosin IIB bundles were less robust in GFP-M5Δ-19× cells (H). The scale bar represents 10 μm.

Fig. 9. GFP-M5Δ expression alters myosin IIB bundles in migrating CHO cells. Non-expressing Di61 (**A–D**), GFP-M5-28× (**E–H**), and GFP-M5Δ-19× (**I–L**) monolayers were wounded (top of each panel), recovered for 6 h and stained with FITC-phalloidin (B,F,J) and anti-myosin IIB (C,G,K). Exposure times for GFP-M5-28× cells were reduced and Di58 exposure times for GFP-M5Δ-19× cells were increased to show bundle detail. In Di61 cells and more so in GFP-M5-28× cells, myosin IIB localizes to robust, straight actin bundles (D,H: merge). In GFP-M5Δ-19× cells, myosin IIB appeared as uniformly distributed speckles (K) that aligned in the direction of thin actin filaments or to larger actin bundles (L, merge). Puncta in (J) represent GFP-M5Δ, not actin aggregates. Scale bar represents 10 μm.

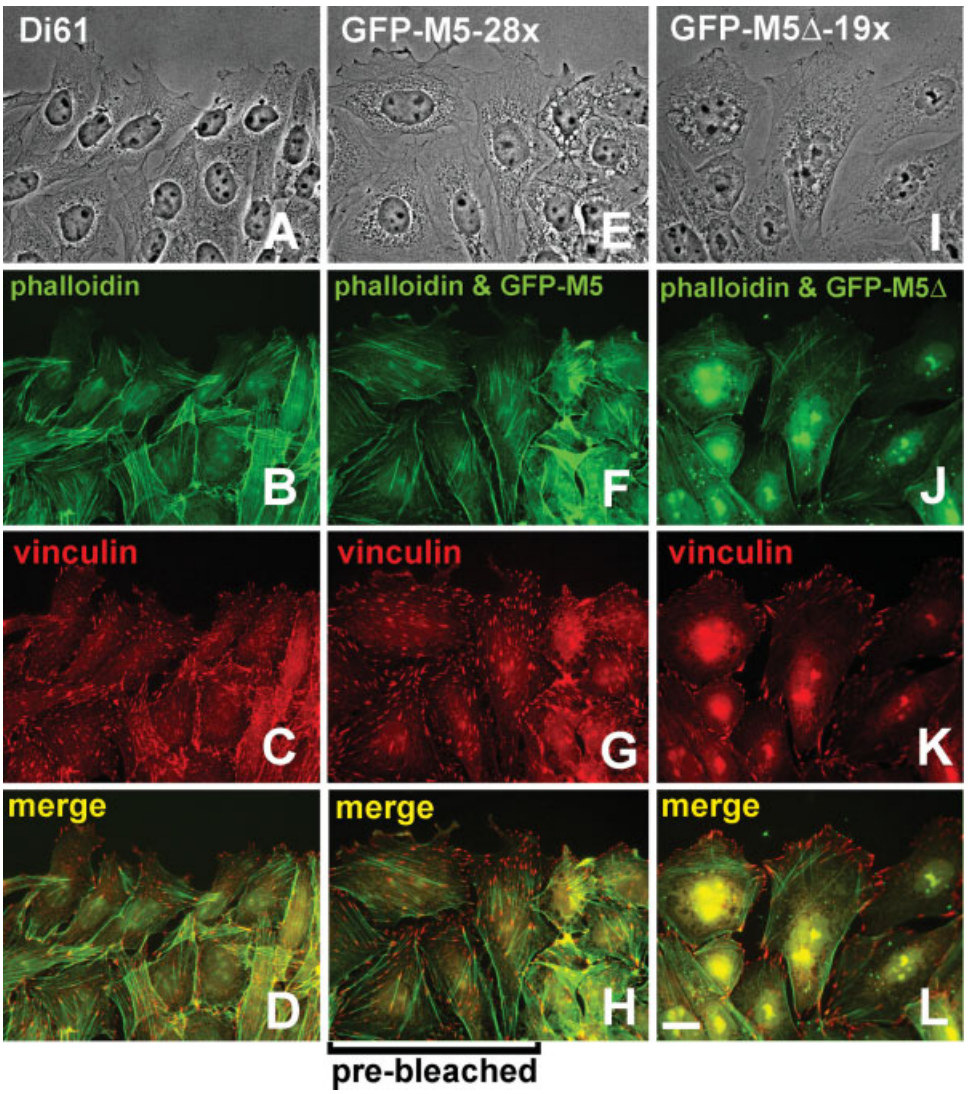

Fig. 10. GFP-M5Δ expression disrupts internal focal adhesions. Non-expressing Di61 (**A**–**D**), GFP-M5-28× (**E**–**H**), and GFP-M5Δ-19× (**I**–**L**) monolayers were wounded (top of each panel), recovered for 6 h, and stained with FITC-phalloidin (B,F,J) and anti-vinculin (C,G,K). Peripheral and internal vinculin-containing focal adhesions are apparent in Di61 cells (C), and more so in GFP-M5-28× cells (G). A robust array of actin fibers (B,F) anchor at focal adhesions (D,H; merge). In contrast, GFP-M5Δ-19× cells lack perinuclear focal adhesions (K) and actin bundles (J). When oriented toward the cell center, peripheral actin bundles begin at a focal adhesion and lack a focal contact internally (L). The diffuse perinuclear vinculin signal in GFP-M5Δ-19× cells is an artifact of the long exposure time needed to acquire images of FITC-phalloidin stained actin stress fibers in GFP-M5Δ-19× cells. Partial bleaching in GFP-M5-28× images (left side) allows visualization of cytoskeleton organization next to the strong phalloidin and vinculin fluorescence (right side). Puncta in (J) represent GFP-M5Δ, not actin aggregates. Scale bar represents 10 μm.

calmodulin) that is involved in myosin Va-induced actin crosslinking, (2) M5Δ is dimerizing with the endogenous CHO myosin Va, forming an unregulated chimeric dimer that has lost actin crosslinking ability, or (3) M5Δ is causing a general effect on the actin cytoskeleton that is unrelated to the function of endogenous myosin Va. At the present time, we do not know whether calmodulin- or myosin light chain 1sa-depletion can occur in the cells expressing high levels of either full length or truncated myosin Va. However, the facts that the full length isoform that we expressed contains all of the same domains as truncated M5Δ, and that expression of full length myosin Va induces, in many cases, opposite phenotypes as M5Δ, argue against the out-competing possibility. Observations that endogenous myosin Va co-immunoprecipitates and co-localizes with GFP-M5Δ in GFP-M5-expressing cells could support the second hypothesis. The unregulated chimeric dimers cannot function properly in GFP-M5Δ-expressing cells. Thus, similar to the cell center accumulation of melanosomes

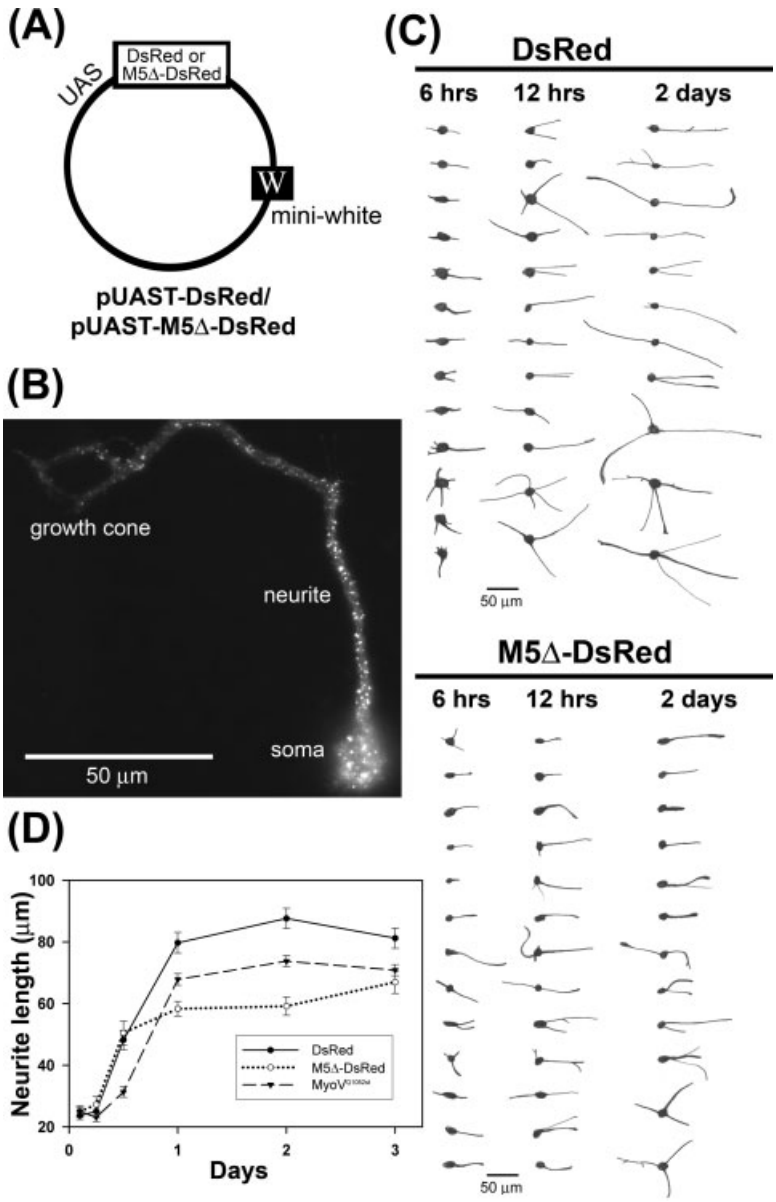

Fig. 11. Expression of M5Δ-DsRed reduces *Drosophila* neurite outgrowth. (**A**) M5Δ sequence was incorporated into a P-element plasmid pUAST that contains a GAL4 –responsive upstream activation sequence (UAS), *mini white* (*w*+) gene, a polylinker site, and the sequence for DsRed, to generate transgenic *Drosophila* lines expressing M5-DsRed or DsRed alone. (**B**) DsRed-M5 localizes as puncta in the cell soma, along neurites, and at the growth cone of *Drosophila* neurons. (**C**) Examples of neurons from DsRed-expressing or M5Δ-DsRed-expressing *Drosophila* embryos, cultured on glass and traced. (**D**). Neurites on neurons cultured from transgenic DsRed-expressing flies, M5Δ-DsRed-expressing flies, or from MyoV^{Q1052st} *Drosophila* that bear a stop codon in the myosin V dimerization domain were measured at 6, 12, 24, 48, and 72 h post-plating. After 2 days in culture, average neurite length for DsRed-expressing neurites (85 μm) was significantly longer than neurites on DsRedM5Δ-expressing (74 μm; $P < 0.0001$) and MyoV^{Q1052st} (65 μm; $P = 0.0009$) neurons (C).

observed in the *dilute* melanocytes, GFP-M5Δ-expressing cells exhibit a perinuclear accumulation of FM4-64 labeled vesicles. However, even if GFP-M5Δ is chelating functional myosin Va, it may also be indirectly producing abnormalities within the actin cytoskeleton. Myosin Va together with GFP-M5Δ moves toward the plus end of actin filaments and could disrupt the stabilization of actin cables which in turn lead to the loss of myosin bundles and focal adhesions. Since studies using antisense, dominant negative tail domains, and *myosin Va*-null cells show that the loss or reduction of functional myosin Va does not eliminate actin bundles, it is likely that the GFP-M5Δ-induced reduction of actin bundles results from general effects of expressing high levels of tailless myosin Va. This is an interesting result because GFP-M5Δ closely resembles a myosin Va cleavage product of calcium-dependent calpain proteases that has been observed in vivo during synaptic activation and excitotoxic injury. This proteolysis leads to cytoskeleton alterations [Casaletti et al., 2003; Alavez et al., 2004]. Indeed we have observed that high expression of truncated mouse myosin V alters actin organization in *Drosophila* neurons, consistent with the hypothesis that mouse heavy meromyosin can induce cytoskeleton rearrangement.

The tail of myosin Va is a better characterized dominant negative. Changes in actin organization have not been reported after tail expression. However, in this

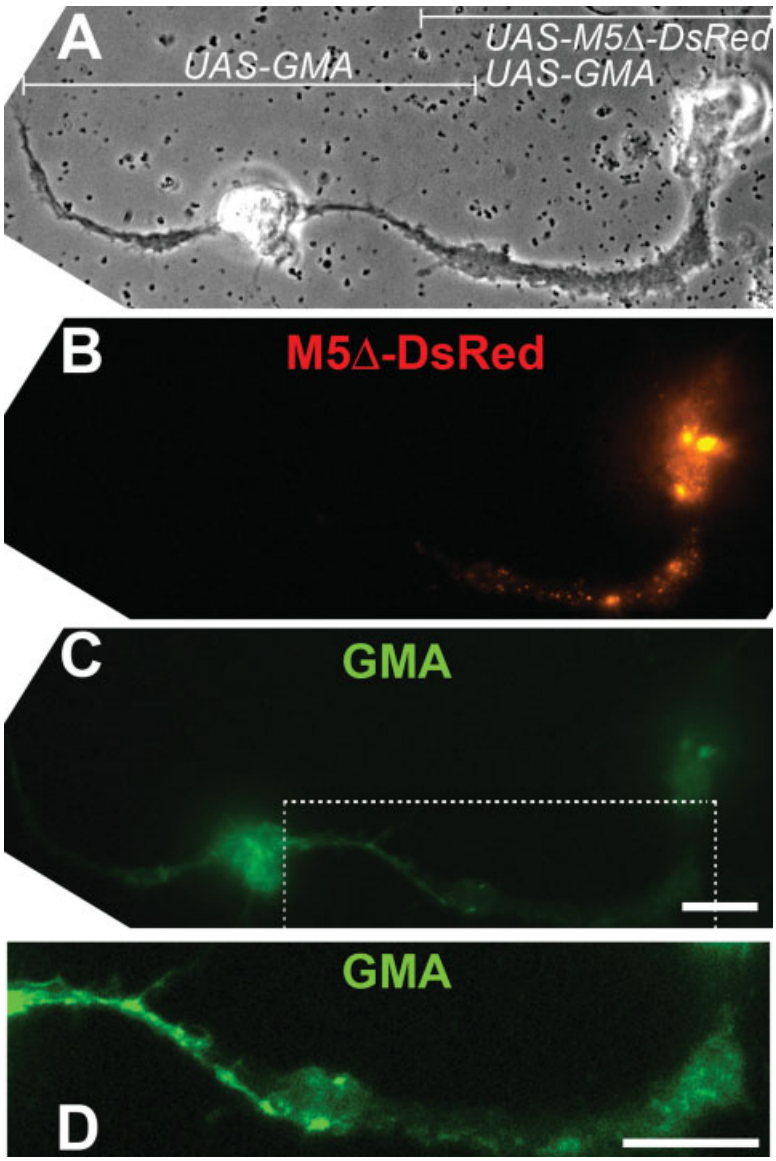

Fig. 12. M5Δ-DsRed reduces F-actin fluorescence intensity and organization in *Drosophila* neurons. (**A**) Phase image of two cultured *Drosophila* neurons that express Gal4. The cell on the left encodes a transgene for Gal4-induced expression of an F-actin marker, GMA (GFP fused to the F-actin binding domain of *Drosophila* moesin). The cell on the right encodes Gal4-inducible transgenes for GMA and M5Δ-DsRed. Gal4 drives expression of M5Δ-DsRed in only the cell on the right (**B**) and GMA in both cells (**C**). GMA fluorescence is less intense in the soma (C) and neurites (**D**, a magnification of C) of the neuron expressing M5Δ-DsRed. Distinct accumulations of GMA that are observed in the neurites of control cells (D, cell on left) are less apparent in neurites expressing M5Δ-DsRed (D, cell on right). Scale bars represent 10 μm.

case, where the tail is thought to out-compete the endogenous myosin Va for its various cargo, we would expect either more inactive myosin Va and perhaps more actin bundling or, if most of the cellular myosin Va is inactive, we would expect no effect on the actin cytoskeleton.

Does myosin Va play a role in cell migration? Our data showing that the expression of tailless mouse myosin Va slows CHO cell migration and *Drosophila* neurite extension, as well as that the $MyoV^{Q1052st}$ mutation reduces *Drosophila* neuron extension, support a role for myosin Va in cellular movement and/or cell morphology. Several lines of evidence also hint for myosin Va at these cellular functions. Myosin Va is localized to the leading edge of cells with highly dynamic membranes [Lionne et al., 2001], to melanocyte dendrites [Nascimento et al., 1997], and to neuronal growth cones [Evans et al., 1997]. The peripheral enrichment of myosin Va can be enhanced by EGF or PDGF stimulation in several cell lines, including NIH-3T3 fibroblasts, human carcinoma A431 cells, and normal rat kidney (NRK) epithelia cells [Buss et al., 1998; Lionne et al., 2001]. Primary melanocytes cultured from *dilute lethal* mice had constricted cell bodies and fewer and thinner dendrites [Wei et al., 1997]. Antisense-mediated decrease of myosin Va reduced the ability of melanocytes to form new dendrites after the cells were replated [Edgar and Bennett, 1999]. Chromophore-assisted laser inactivation inhibited the ability of myosin Va to translocate actin filaments in vitro and decreased the rate of filopodial extension in chick dorsal root ganglion cells [Wang et al., 1996]. In the *dilute-neurological* mice that express low levels of the N-terminal fragment of myosin Va resulting in a

neurological defect, climbing fibers fail to extend fully through the molecular layer of the cerebellum and to form appropriate synapses with Purkinje cells [Takagishi et al., 2007]. Therefore, it is possible that myosin Va participates in cellular functions, such as cytoskeleton regulation and vesicle transport, that support cell motility.

That being said, it is unlikely that myosin Va activity is indispensable in cell migration in vivo. Such a conclusion contrasts with a number of studies that show that aberrant vesicular traffic, rather than a gross motility defect, underlies the phenotypes observed in mice bearing myosin Va mutations. *Dilute lethal* melanocytes form dendrites in culture and in situ [Provance et al., 1996; Wei et al., 1997]. Superior cervical ganglion neurons, explanted from the *dilute lethal* mice, have no discernable difference in growth cone shape, average neurite length, maximum filopodial length, or actin organization, compared to SCGs that express myosin Va [Evans et al., 1997]. The most convincing evidence is that *dilute lethal* mice display no gross morphological defects and melanocyte precursors migrate normally from the neural crest to the skin [Mercer et al., 1991; Jackson, 1994]. Similarly, *Drosophila* $MyoV^{Q1052st}$ larva develop normally until 3 days after hatching [Mermall et al., 2005]. Therefore, if myosin Va plays a role in cell migration it is likely to be a subtle role that can, in situ, be compensated for by other mechanisms.

ACKNOWLEDGMENTS

The authors thank N.A. Jenkins, J.A. Hammer III, M.A. Shea, W.A. Johnson, R.S. Walikonis, J.A. Mercer, M.S. Mooseker, and L. Cooley for reagents and fly lines; Wenjia Chen, Wei-Hua Lee, Jihye Lee, A. Van Winkle, J. Keller, D. Dallon, and the D.R. Soll Keck Facility team for technical assistance.

REFERENCES

Alavez S, Moran J, Franco-Cea A, Ortega-Gomez A, Casaletti L, Cameron LC. 2004. Myosin Va is proteolysed in rat cerebellar granule neurons after excitotoxic injury. Neurosci Lett 367(3): 404–409.

Andersen R, Li Y, Resseguie M, Brenman JE. 2005. Calcium/calmodulin-dependent protein kinase II alters structural plasticity and cytoskeletal dynamics in *Drosophila*. J Neurosci 25(39):8878–8888.

Bloor JW, Kiehart DP. 2001. Zipper nonmuscle myosin-II functions downstream of PS2 integrin in *Drosophila* myogenesis and is necessary for myofibril formation. Dev Biol 239(2):215–228.

Bridgman PC. 1999. Myosin Va movements in normal and dilute-lethal axons provide support for a dual filament motor complex. J Cell Biol 146(5):1045–1060.

Buss F, Kendrick-Jones J, Lionne C, Knight AE, Cote GP, Paul Luzio J. 1998. The localization of myosin VI at the golgi complex and leading edge of fibroblasts and its phosphorylation and recruitment into membrane ruffles of A431 cells after growth factor stimulation. J Cell Biol 143(6):1535–1545.

Cai Y, Biais N, Giannone G, Tanase M, Jiang G, Hofman JM, Wiggins CH, Silberzan P, Buguin A, Ladoux B, Sheetz MP. 2006. Nonmuscle myosin IIA-dependent force inhibits cell spreading and drives F-actin flow. Biophys J 91(10):3907–3920.

Cao TT, Chang W, Masters SE, Mooseker MS. 2004. Myosin-Va binds to and mechanochemically couples microtubules to actin filaments. Mol Biol Cell 15(1):151–161.

Casaletti L, Tauhata SB, Moreira JE, Larson RE. 2003. Myosin-Va proteolysis by Ca^{2+}/calpain in depolarized nerve endings from rat brain. Biochem Biophys Res Commun 308(1):159–164.

Cheney RE, O'Shea MK, Heuser JE, Coelho MV, Wolenski JS, Espreafico EM, Forscher P, Larson RE, Mooseker MS. 1993. Brain myosin-V is a two-headed unconventional myosin with motor activity. Cell 75(1):13–23.

Dekker-Ohno K, Hayasaka S, Takagishi Y, Oda S, Wakasugi N, Mikoshiba K, Inouye M, Yamamura H. 1996. Endoplasmic reticulum is missing in dendritic spines of Purkinje cells of the ataxic mutant rat. Brain Res 714:226–230.

Dutta D, Bloor JW, Ruiz-Gomez M, VijayRaghavan K, Kiehart DP. 2002. Real-time imaging of morphogenetic movements in *Drosophila* using Gal4-UAS-driven expression of GFP fused to the actin-binding domain of moesin. Genesis 34(1/2):146–151.

Edgar AJ, Bennett JP. 1999. Inhibition of dendrite formation in mouse melanocytes transiently transfected with antisense DNA to myosin Va. J Anat 195 (Part 2):173–184.

Edwards KA, Demsky M, Montague RA, Weymouth N, Kiehart DP. 1997. GFP-moesin illuminates actin cytoskeleton dynamics in living tissue and demonstrates cell shape changes during morphogenesis in *Drosophila*. Dev Biol 191(1):103–117.

Eppinga RD, Li Y, Lin JL-C, Lin JJ-C. 2006a. Tropomyosin and caldesmon regulate cytokinesis speed and membrane stability during cell division. Arch Biochem Biophys 456(2):161–174.

Eppinga RD, Li Y, Lin JL-C, Mak AS, Lin JJ-C. 2006b. Requirement of reversible caldesmon phosphorylation at P21-activated kinase-responsive sites for lamellipodia extensions during cell migration. Cell Motil Cytoskeleton 63(9):543–562.

Espindola FS, Suter DM, Partata LB, Cao T, Wolenski JS, Cheney RE, King SM, Mooseker MS. 2000. The light chain composition of chicken brain myosin-Va: Calmodulin, myosin-II essential light chains, and 8-kDa dynein light chain/PIN. Cell Motil Cytoskeleton 47(4):269–281.

Espreafico EM, Cheney RE, Matteoli M, Nascimento AA, De Camilli PV, Larson RE, Mooseker MS. 1992. Primary structure and cellular localization of chicken brain myosin-V (p190), an unconventional myosin with calmodulin light chains. J Cell Biol 119(6):1541–1557.

Evans LL, Hammer J, Bridgman PC. 1997. Subcellular localization of myosin V in nerve growth cones and outgrowth from dilute-lethal neurons. J Cell Sci 110 (Part 4):439–449.

Evans LL, Lee AJ, Bridgman PC, Mooseker MS. 1998. Vesicle-associated brain myosin-V can be activated to catalyze actin-based transport. J Cell Sci 111 (Part 14):2055–2066.

Hegmann TE, Lin JL-C, Lin JJ-C. 1989. Probing the role of nonmuscle tropomyosin isoforms in intracellular granule movement by microinjection of monoclonal antibodies. J Cell Biol 109(3):1141–1152.

Huang JD, Brady ST, Richards BW, Stenolen D, Resau JH, Copeland NG, Jenkins NA. 1999. Direct interaction of microtubule- and actin-based transport motors. Nature 397(6716):267–270.

Jackson IJ. 1994. Molecular and developmental genetics of mouse coat color. Annu Rev Genet 28:189–217.

Krementsov DN, Krementsova EB, Trybus KM. 2004. Myosin V: Regulation by calcium, calmodulin, and the tail domain. J Cell Biol 164(6):877–886.

Langford GM. 2002. Myosin-V, a versatile motor for short-range vesicle transport. Traffic 3(12):859–865.

Li BX, Satoh AK, Ready DF. 2007. Myosin V, Rab11, and dRip11 direct apical secretion and cellular morphogenesis in developing *Drosophila* photoreceptors. J Cell Biol 177(4):659–669.

Li XD, Mabuchi K, Ikebe R, Ikebe M. 2004a. Ca^{2+}-induced activation of ATPase activity of myosin Va is accompanied with a large conformational change. Biochem Biophys Res Commun 315(3): 538–455.

Li Y, Lin JL-C, Reiter RS, Daniels K, Soll DR, Lin JJ-C. 2004b. Caldesmon mutant defective in Ca^{2+}/calmodulin binding interferes with assembly of stress fibers and affects cell morphology, growth and motility. J Cell Sci 117 (Part 16):3593–3604.

Lionne C, Buss F, Hodge T, Ihrke G, Kendrick-Jones J. 2001. Localization of myosin Va is dependent on the cytoskeletal organization in the cell. Biochem Cell Biol 79(1):93–106.

Liu J, Taylor DW, Krementsova EB, Trybus KM, Taylor KA. 2006. Three-dimensional structure of the myosin V inhibited state by cryoelectron tomography. Nature 442(7099):208–211.

Lo CM, Buxton DB, Chua GC, Dembo M, Adelstein RS, Wang YL. 2004. Nonmuscle myosin IIb is involved in the guidance of fibroblast migration. Mol Biol Cell 15(3):982–989.

Mercer JA, Seperack PK, Strobel MC, Copeland NG, Jenkins NA. 1991. Novel myosin heavy chain encoded by murine dilute coat colour locus. Nature 349(6311):709–713.

Mermall V, Bonafe N, Jones L, Sellers JR, Cooley L, Mooseker MS. 2005. Drosophila myosin V is required for larval development and spermatid individualization. Dev Biol 286(1):238–255.

Miller KE, Sheetz MP. 2000. Characterization of myosin V binding to brain vesicles. J Biol Chem 275(4):2598–2606.

Nascimento AA, Amaral RG, Bizario JC, Larson RE, Espreafico EM. 1997. Subcellular localization of myosin-V in the B16 melanoma cells, a wild-type cell line for the dilute gene. Mol Biol Cell 8(10):1971–1988.

Pastural E, Barrat FJ, Dufourcq-Lagelouse R, Certain S, Sanal O, Jabado N, Seger R, Griscelli C, Fischer A, de Saint Basile G. 1997. Griscelli disease maps to chromosome 15q21 and is associated with mutations in the myosin-Va gene. Nat Genet 16(3):289–292.

Peng IF, Wu CF. 2007. Differential contributions of Shaker and Shab K^+ currents to neuronal firing patterns in *Drosophila*. J Neurophysiol 97(1):780–794.

Prekeris R, Terrian DM. 1997. Brain myosin V is a synaptic vesicle-associated motor protein: Evidence for a Ca^{2+}-dependent interaction with the synaptobrevin-synaptophysin complex. J Cell Biol 137(7):1589–1601.

Provance DW, Jr., Wei M, Ipe V, Mercer JA. 1996. Cultured melanocytes from dilute mutant mice exhibit dendritic morphology and altered melanosome distribution. Proc Natl Acad Sci USA 93(25):14554–14558.

Provance DW, Mercer JA. 1999. Myosin-V: head to tail. Cell Mol Life Sci 56(3/4):233–242.

Rao MV, Engle LJ, Mohan PS, Yuan A, Qiu D, Cataldo A, Hassinger L, Jacobsen S, Lee VM, Andreadis A, Julien JP, Bridgman PC, Nixon RA. 2002. Myosin Va binding to neurofilaments is essential for correct myosin Va distribution and transport and neurofilament density. J Cell Biol 159(2):279–290.

Reck-Peterson SL, Provance DW, Jr., Mooseker MS, Mercer JA. 2000. Class V myosins. Biochim Biophys Acta 1496(1):36–51.

Rudolf R, Kogel T, Kuznetsov SA, Salm T, Schlicker O, Hellwig A, Hammer JA, III, Gerdes HH. 2003. Myosin Va facilitates the distribution of secretory granules in the F-actin rich cortex of PC12 cells. J Cell Sci 116 (Part 7):1339–1348.

Saito M, Wu CF. 1991. Expression of ion channels and mutational effects in giant *Drosophila* neurons differentiated from cell division-arrested embryonic neuroblasts. J Neurosci 11(7):2135–2150.

Searle AG. 1952. A lethal allele of dilute in the house mouse. Heredity 6:395.

Soll DR. 1995. The use of computers in understanding how animal cells crawl. Int Rev Cytol 8:439–454.

Soll DR, Voss E. 1998. Two and three-dimensional computer systems for analyzing how cells crawl. In: Soll DR, Wessels D, editors. Motion analysis of living cells. New York: Wiley-Liss. p 25–52.

Tabb JS, Molyneaux BJ, Cohen DL, Kuznetsov SA, Langford GM. 1998. Transport of ER vesicles on actin filaments in neurons by myosin V. J Cell Sci 111 (Part 21):3221–3234.

Takagishi Y, Murata Y. 2006. Myosin Va mutation in rats is an animal model for the human hereditary neurological disease, Griscelli syndrome type 1. Ann N Y Acad Sci 1086:66–80.

Takagishi Y, Hashimoto K, Kayahara T, Watanabe M, Otsuka H, Mizoguchi A, Kano M, Murata Y. 2007. Diminished climbing fiber innervation of Purkinje cells in the cerebellum of myosin Va mutant mice and rats. Dev Neurobiol 67(7):909–923.

Tauhata SB, dos Santos DV, Taylor EW, Mooseker MS, Larson RE. 2001. High affinity binding of brain myosin-Va to F-actin induced by calcium in the presence of ATP. J Biol Chem 276(43):39812–39818.

Wakatsuki T, Wysolmerski RB, Elson EL. 2003. Mechanics of cell spreading: role of myosin II. J Cell Sci 116 (Part 8):1617–1625.

Walikonis RS, Jensen ON, Mann M, Provance DW, Jr., Mercer JA, Kennedy MB. 2000. Identification of proteins in the postsynaptic density fraction by mass spectrometry. J Neurosci 20(11): 4069–4080.

Wang F, Chen L, Arcucci O, Harvey EV, Bowers B, Xu Y, Hammer JA, III, Sellers JR. 2000. Effect of ADP and ionic strength on the kinetic and motile properties of recombinant mouse myosin V. J Biol Chem 275(6):4329–4335.

Wang F, Thirumurugan K, Stafford WF, Hammer JA, III, Knight PJ, Sellers JR. 2004. Regulated conformation of myosin V. J Biol Chem 279(4):2333–2336.

Wang FS, Wolenski JS, Cheney RE, Mooseker MS, Jay DG. 1996. Function of myosin-V in filopodial extension of neuronal growth cones. Science 273(5275):660–663.

Warren KS, Lin JL-C, Wamboldt DD, Lin JJ-C. 1994. Overexpression of human fibroblast caldesmon fragment containing actin-, Ca^{2+}/calmodulin-, and tropomyosin-binding domains stabilizes endogenous tropomyosin and microfilaments. J Cell Biol 125(2):359–368.

Warren KS, Lin JL-C, McDermott JP, Lin JJ-C. 1995. Forced expression of chimeric human fibroblast tropomyosin mutants affects cytokinesis. J Cell Biol 129:697–708.

Waterman-Storer C, Duey DY, Weber KL, Keech J, Cheney RE, Salmon ED, Bement WM. 2000. Microtubules remodel actomyosin networks in Xenopus egg extracts via two mechanisms of F-actin transport. J Cell Biol 150(2):361–376.

Wei Q, Wu X, Hammer JA, III. 1997. The predominant defect in dilute melanocytes is in melanosome distribution and not cell shape, supporting a role for myosin V in melanosome transport. J Muscle Res Cell Motil 18(5):517–527.

Wu CF, Sakai K, Saito M, Hotta Y. 1990. Giant *Drosophila* neurons differentiated from cytokinesis-arrested embryonic neuroblasts. J Neurobiol 21(3):499–507.

Wu X, Bowers B, Wei Q, Kocher B, Hammer JA, III. 1997. Myosin V associates with melanosomes in mouse melanocytes: Evidence

that myosin V is an organelle motor. J Cell Sci 110 (Part 7):847–859.

Wu X, Bowers B, Rao K, Wei Q, Hammer JAr. 1998a. Visualization of melanosome dynamics within wild-type and dilute melanocytes suggests a paradigm for myosin V function In vivo. J Cell Biol 143(7):1899–1918.

Wu X, Kocher B, Wei Q, Hammer JA, III. 1998b. Myosin Va associates with microtubule-rich domains in both interphase and dividing cells. Cell Motil Cytoskeleton 40(3):286–303.

Wu X, Wang F, Rao K, Sellers JR, Hammer JA, III. 2002. Rab27a is an essential component of melanosome receptor for myosin Va. Mol Biol Cell 13(5):1735–1749.

Wu XS, Tsan GL, Hammer JA, III. 2005. Melanophilin and myosin Va track the microtubule plus end on EB1. J Cell Biol 171(2):201–207.

Wylie SR, Wu PJ, Patel H, Chantler PD. 1998. A conventional myosin motor drives neurite outgrowth. Proc Natl Acad Sci USA 95(22): 12967–12972.

Yao WD, Wu CF. 1999. Auxiliary hyperkinetic β subunit of K^+ channels: Regulation of firing properties and K^+ currents in *Drosophila* neurons. J Neurophysiol 81(5):2472–2484.

Yao WD, Rusch J, Poo M, Wu CF. 2000. Spontaneous acetylcholine secretion from developing growth cones of *Drosophila* central neurons in culture: Effects of cAMP-pathway mutations. J Neurosci 20(7):2626–2637.